Synthesis of classes of ternary metal oxide nanostructures

Yuanbing Mao,[a] Tae-Jin Park[a] and Stanislaus S. Wong*[ab]

Received (in Cambridge, UK) 14th July 2005, Accepted 15th September 2005
First published as an Advance Article on the web 3rd November 2005
DOI: 10.1039/b509960a

Nanoscale structures, such as nanoparticles, nanorods, nanowires, nanocubes, and nanotubes, have attracted extensive synthetic attention as a result of their novel size-dependent properties. Ideally, the net result of nanoscale synthesis is the production of structures that achieve monodispersity, stability, and crystallinity with a predictable morphology. Many of the synthetic methods used to attain these goals have been based on principles derived from semiconductor technology, solid state chemistry, and molecular inorganic cluster chemistry. We describe a number of advances that have been made in the reproducible synthesis of various ternary oxide nanomaterials, including alkaline earth metal titanates, alkali metal titanates, bismuth ferrites, ABO_4-type oxides, as well as miscellaneous classes of ternary metal oxides.

1. Introduction

The family of nanomaterials, *i.e.* structures with at least one dimension between 1 nm and 100 nm, includes a host of substances, such as nanoparticles, nanocubes, nanorods, nanobelts, nanosheets, nanowires, and nanotubes.[1–9] They are fundamentally interesting due to their fascinating size-dependent optical, electronic, magnetic, thermal, mechanical, and chemical properties, which are distinct from their bulk counterparts as well as from the atomic or molecular precursors from whence they were derived. From the point of view of applications in areas ranging from energy storage, fuel cells, nanomedicine, molecular computing, nanophotonics, tunable resonant devices, catalysis, and sensing, it is widely believed that nanoscale materials possess intriguing properties that are comparable to or superior to those of bulk.[10,11]

For instance, one-dimensional (1-D) nanomaterials with their inherent anisotropy are the smallest dimension structures that can be used for the efficient transport of electrons and optical excitations.[12–17] As such, they are applicable as building blocks for the assembly of the next generation of molecular electronic and computational devices, equipped with high-density information storage. To carefully study and exploit the potential and possibilities associated with nanomaterials, the key point is to create well-defined, monodisperse structures of predictable size, shape, crystallinity, and morphology through a straightforward synthesis. Most importantly, from our perspective as chemists, these materials need to be controllably generated with a reliable and reproducible chemical protocol to deliver high quantities and yields with an exceptional degree of purity. It is critical to attain these objectives as the creation of novel, functional systems with

[a]*Department of Chemistry, State University of New York at Stony Brook, Stony Brook, NY 11794, USA. E-mail: sswong@notes.cc.sunysb.edu; Tel: +1 631 632 1703*
[b]*Materials and Chemical Sciences Department, Brookhaven National Laboratory, Building 480, Upton, NY 11973, USA. E-mail: sswong@bnl.gov; Tel: +1 631 344 3178*

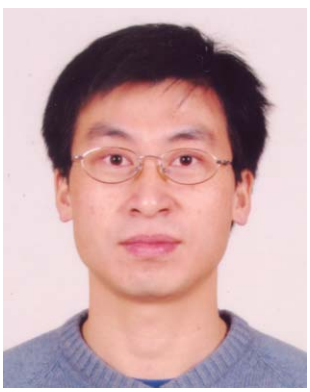

Yuanbing Mao

Yuanbing Mao was born in Hunan, China. He received his BSc from Xiangtan University in Hunan, China in 1997 and his MSc from the Institute of Chemistry, Chinese Academy of Sciences in Beijing, China in 2000 under the supervision of Prof. Bizhong Li and Prof. Qing Yan. Currently, he is a doctoral student under the supervision of Prof. Stanislaus S. Wong in the Department of Chemistry at the State University of New York at Stony Brook. His research interests are in the areas of the design, synthesis, and characterization of metal oxide nanomaterials and their associated applications. He received a Sigma Xi Grant-in-Aid of Research in 2004 and a Sigma Xi Travel Award in 2005.

Tae-Jin Park

Tae-Jin Park was born in Seoul, Korea. He earned BSc and MSc degrees in Chemistry from Yonsei University in 1997 and 1999, respectively. After completing compulsory military service in 2001, he worked as a research scientist at the Korea Institute Science Technology (KIST). He is currently pursuing a PhD degree in the Department of Chemistry at the State University of New York under the supervision of Prof. Stanislaus S. Wong. His research interests include the structural characterization of carbon nanotubes as well as the synthesis and characterization of nanoscale functional materials, such as metal oxide nanomaterials.

desirable properties often relies on taking advantage of complementary interconnectivity amongst the various nanoscale components.

Many of the synthetic methods used to attain these goals have been based on principles derived from semiconductor technology, solid state chemistry, and molecular inorganic cluster chemistry. The most popular techniques[4,10,18–23] include nanostructure formation through a *chimie douce* solution chemistry methodology, a sol-gel processing mechanism, the use of microemulsions, the utilization of hydrothermal and solvothermal methods, the kinetic control of growth through the use of capping reagents, the application of template-inspired methodologies, and lastly, biomimetic syntheses.

To date, much of the synthetic effort has been directed toward the generation of carbon nanostructures and semiconducting quantum dot-type nanostructures. Metal oxides, in particular, represent one of the most diverse classes of materials, with important structure-related properties. Many exhibit superconductivity, ferroelectricity, magnetism, colossal magnetoresistivity, conductivity, and/or gas-sensing capabilities. It is evident that the synthesis of metal oxide nanostructures will lead to key developments in the construction of devices.

Specifically, comparatively little work has been performed on the fabrication of technologically important ternary metal oxide nanostructures, which has hindered detailed experimental investigations on the size-dependent properties of these oxide materials. Developing approaches to prepare and scale up new synthetic formulations of these oxide nanostructures has been the recent focus of our efforts.

While there are a few existing review articles concerning the synthesis of non-carbonaceous nanomaterials,[3,12,14,24–26] these tend to focus on metallic, semiconducting, and/or binary oxide nanoparticles. In the current manuscript, we discuss recent advances in the synthesis of various ternary oxide nanomaterials with a particular emphasis on perovskite materials and with a special focus on efforts in our group. Specifically, we initially consider alkaline earth metal titanates (Section 2), proceed with a discussion of alkali metal titanates (Section 3), deal with bismuth ferrites (Section 4), consider ABO_4-type oxides (Section 5), and lastly, conclude with a reflection on a broad range of other classes of ternary oxide materials (Section 6). Hence, in each section of this review, we focus on a particular class of ternary oxide nanomaterials, highlight its importance and industrial applicability, and then proceed to discuss recent advances in their rational synthesis. A summary and outlook of this review is given in Section 7.

Stanislaus S. Wong

Stanislaus S. Wong earned a BSc (First Class Honours) from McGill University in 1994 and subsequently completed his PhD thesis from Harvard University in 1999 under the tutelage of Professor Charles M. Lieber. After finishing a postdoctoral fellowship at Columbia University with Professor Louis E. Brus, he has held the position of Assistant Professor in Chemistry at the State University of New York at Stony Brook with a joint appointment at Brookhaven National Laboratory, since September 2000. He and his group have wide-ranging interests in nanotechnology, including the rational chemical functionalization of carbon nanotubes, the synthesis and characterization of metal oxide nanostructures (such as perovskites), the development of synchrotron-based techniques for nanoscale characterization, and the use of probe microscopy to initiate localized chemistry. Professor Wong has been a 3M non-tenured faculty fellow since 2002 and earned a National Science Foundation CAREER award, commencing in 2004.

2. Nanostructures of alkaline earth metal titanates

2.1. Introduction

Alkaline earth metal titanates, including $BaTiO_3$, $SrTiO_3$, $CaTiO_3$, and their associated non-stoichiometric complexes, (Ca, Sr, Ba)TiO_3, are important ferroelectric perovskite materials. In general, ferroelectric materials possess a low symmetry which gives rise to a spontaneous polarization along one or more crystal axes.[27] Thermodynamically stable, these different polarization states can be switched from one to the other by the application of an external field known as the coercive field, E_c. This intrinsic ability of ferroelectric materials to switch their polarization direction between two stable polarized states provides the basis for binary code-based non-volatile ferroelectric random-access memories (NVFRAMs). Compared with bulk ferroelectrics, low-dimensional nanoscale ferroelectric structures may increase the storage density of NVFRAMs by as much as a factor of 5.[28] These anticipated benefits hinge on whether phase transitions and multi-stable states still exist in low-dimensional systems, such as nanoparticles and nanorods.

Specifically, ferroelectric perovskite-type oxides, with a general formula of ABO_3, are noteworthy for their advantageous dielectric, piezoelectric, electrostrictive, pyroelectric, and electro-optic properties with corresponding applications in the electronics industry for transducers, actuators, and high-k-dielectrics.[29–31] Understanding the behavior of and the preparation of these ferroelectric materials with structure-dependent physical properties, at the nanoscale, are of importance to the development of molecular electronics.[31–33] In particular, these materials find applications in non-volatile memory, dynamic random access memory (DRAM), field-effect transistors, electro-optic devices, electromechanical devices, and logic circuitry.[34,35] In particular, ferroelectric nanotubes made of oxide insulators have a variety of applications in terms of pyroelectric detectors, piezoelectric ink-jet printers, fluidic devices, and memory capacitors, which cannot necessarily be fulfilled by nanotubes created from other materials.

2.2. Nanoscale perovskite production—barium titanate and strontium titanate

Ferroelectric perovskite oxides, including $BaTiO_3$ and $SrTiO_3$, exhibit large non-linear optical coefficients and large dielectric constants.[36–38] Their novel physical properties often result

from strong electron–electron interactions. Because these effects are dependent on structure and finite size (*e.g.* the ferroelectric transition temperature of isolated grains may decrease for average grain parameters of about 200 nm),[38,39] considerable effort has been expended in the controllable synthesis of crystalline materials and of thin films of these ferroelectric oxides. In view of the scientific importance of these materials, it is not surprising that a wide variety of approaches aimed at their nanoscale synthesis have been reported.

Previous work in synthesizing these materials has been associated with a number of different routes.[40] For instance, free-standing 10–30 nm nanoparticle films of Pb(Zr, Ti)O_3 (PZT) have been prepared by a modified sol-gel method.[41] Monodisperse nanoparticles of barium titanate, with diameters ranging from 6 to 12 nm, have been synthesized through a generalized injection-hydrolysis procedure.[42] In addition, well-isolated $BaTiO_3$ and $SrTiO_3$ nanorods with diameters ranging from 5 to 60 nm and lengths reaching up to 10 microns have been prepared by the solution-phase decomposition of bimetallic alkoxide precursors in the presence of coordinating ligands (Fig. 1).[43,44] Scanning probe

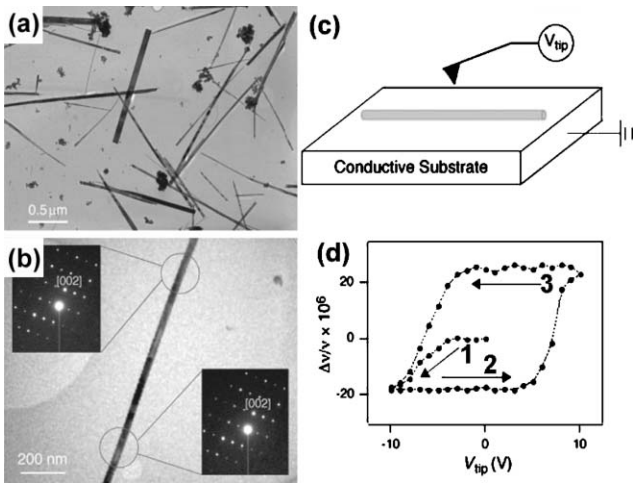

Fig. 1 (a) Transmission electron microscopy (TEM) image of $BaTiO_3$ nanowires, showing that the reaction produces mostly nanowires and minor quantities ($\sim$10%) of nanoparticle aggregates. (b) TEM image of a 30 nm diameter $BaTiO_3$ nanowire along with two convergent beam electron diffraction (CBED) patterns shown as insets. The circles represent the region where the CBED patterns are obtained. Analysis of the CBED patterns shows that the nanowire is single crystalline with the [100] direction aligned along the wire axis. (c) Schematic diagram illustrating the experimental geometry for reading and writing local areas of polarization of a nanowire. (d) Plot of the fractional shift in the cantilever resonance frequency [$\Delta v/v = (v_0 - v)/v_0$] as a function of the writing voltage (V_{tip}) that illustrates a hysteresis behavior of polarization switching. The electrostatic force felt by the tip and hence the magnitude of electric polarization on the nanowire is directly proportional to $\Delta v/v$. Each data point in the plot was obtained by applying the writing voltage for 3 min and subsequently measuring the shift in the cantilever resonance frequency at $V_{tip} = -2$ V. The V_{tip} scan sequence was from 0 to -10 V (arrow 1), -10 V to +10 V (arrow 2), and +10 V to -10 V (arrow 3). The distance between the tip and the top surface of the nanowire was 10 nm during the writing procedure and 35 nm during the reading procedure. Reprinted with permission from reference 44. Reproduced with permission of Wiley-VCH.

investigations[45] later showed that non-volatile electric polarization could be reproducibly induced and manipulated on these nanowires and nanorods, thereby demonstrating that nanowires as small as 10 nm in diameter could retain ferroelectricity (Fig. 1).

A low temperature direct synthesis (LTDS) method[46] between Ba and Ti ions was established to synthesize $BaTiO_3$ crystallites with particle sizes of around 10 nm; synthetic conditions for barium titanate formation involved temperatures greater than 50 °C and Ba:Ti atomic ratios higher than 5:1. Very recently, a non-aqueous route[47] to the preparation of nanocrystalline $BaTiO_3$, $SrTiO_3$, and (Ba, Sr)TiO_3 nanoparticles in the sub-10 nm size range has been developed (Fig. 2). In this procedure,

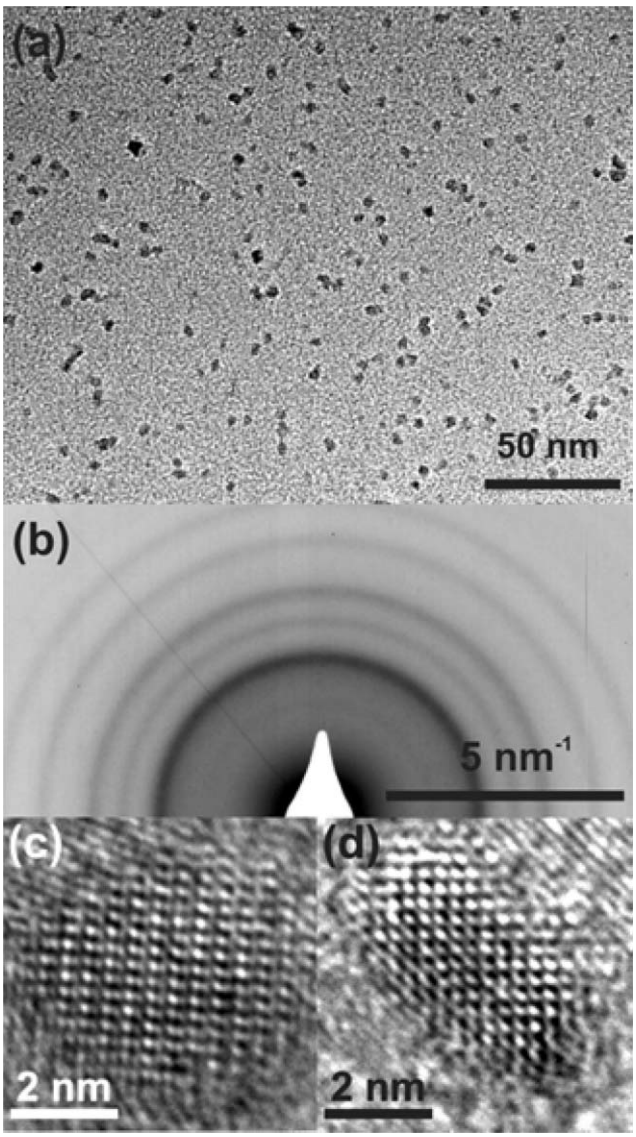

Fig. 2 Representative TEM micrographs of as-synthesized $BaTiO_3$ nanoparticles. (a) An overview image proves the exclusive presence of $BaTiO_3$ nanoparticles without the presence of larger particles or agglomerates; (b) selected area electron diffraction (SAED) pattern; (c) and (d) high-resolution TEM (HRTEM) images of isolated $BaTiO_3$ nanocrystals. Reprinted with permission from M. Niederberger, G. Garnweitner, N. Pinna, and M. Antonietti, *J. Am. Chem. Soc.*, 2004 **126**, 9120. Copyright 2004 American Chemical Society.

a one-pot reaction process, elemental alkaline earth metals are directly dissolved in benzyl alcohol at slightly elevated temperatures. After the addition of titanium(IV) isopropoxide, the reaction mixture is heated to 200 °C, resulting in the formation of crystalline product, which is believed to be produced mainly *via* a novel pathway involving C–C bond formation between benzyl alcohol and an isopropanolate ligand.

$BaTiO_3$ and $PbTiO_3$ nanotubes, with an outer diameter of 200 nm and a length of up to 50 microns, have been prepared using a sol-gel template methodology, which produces aggregated "spaghetti-like" tangles (Fig. 3).[48] Others have reported several different, analogous deposition techniques, including misted chemical solution deposition and uniform pore wetting of porous alumina templates[48] or macroporous silicon, to fabricate ferroelectric nanotubes of various compositions with structures as small as 20 nm.[48–51] Template techniques have also been used to fabricate core-shell nanowires of $PbZr_{0.52}Ti_{0.48}O_3$ with diameters ranging from 50 nm to several microns and with lengths over 100 microns; this synthesis was performed through an epitaxial deposition of the desired transition metal oxides onto vertically aligned, ordered arrays of single-crystalline MgO nanowires.[52]

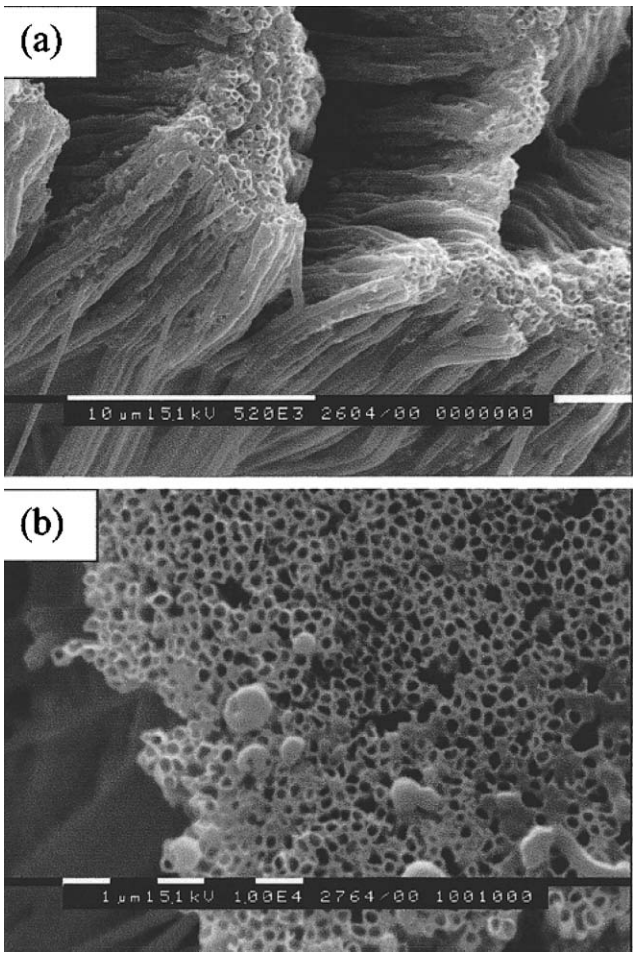

Fig. 3 Scanning electron microscopy (SEM) images of perovskite nanotubes formed during sol-gel template synthesis using 200 nm alumina template membranes. (a) Side view showing bundle formation after the removal of the template. (b) Top view of $PbTiO_3$ bundle illustrating formation of open tubes with an outer diameter of 200 nm. With both materials, the nanotubes are 50 μm in length, which is the thickness of the template membrane. Reprinted with permission from reference 48. Copyright 2002 American Chemical Society.

Hydrothermal media[53–57] provide an effective reaction environment for the synthesis of numerous ceramic materials because of the combined effects of solvent, temperature, and pressure on ionic reaction equilibria. In particular, the properties of phase-pure ceramic powders can be controlled by varying temperature, pressure, reactant concentrations, pH, and other similar variables. Lu *et al.*[58] have synthesized $BaTiO_3$ nanocrystals measuring 78 to 83 nm using a hydrothermal method in the presence of Tween 80 surfactant at 230 °C for 0.5 to 2 h. In fact, in our group, small, isolated crystalline $BaTiO_3$ and $SrTiO_3$ nanotubes with an inner diameter of ~4 nm, an outer diameter of ~8 nm, and a length of about several hundred nanometres have been assembled through a low-temperature hydrothermal reaction by using titanium oxide nanotubes as a *bona fide* precursor material.[59] Han *et al*. recently described[60] the growth of single-crystalline tetragonal perovskite $PbZr_{0.52}Ti_{0.48}O_3$ nanorods and nanowires by a hydrothermal process, assisted by poly(acrylic acid) and poly(vinyl alcohol).

2.3. Molten salt synthesis of barium titanate, strontium titanate, and calcium strontium titanate nanomaterials

The majority of these aforementioned methods yield relatively small quantities of the desired nanostructures, and furthermore, in most cases, extremely toxic, expensive, and unstable organometallic precursors are also employed. Thus, the development of gram-scale and environmentally benign synthetic methods with reproducible shape control is of paramount importance if the full potential of these materials is to be realized.

To this end, a large-scale and facile solid-state reaction by a molten salt process has been proposed[61] by our group as a means of preparing single-crystalline $BaTiO_3$ and $SrTiO_3$ nanostructures in an NaCl medium at 820 °C in the presence of a non-ionic surfactant. In a typical synthesis, barium or strontium oxalate (depending on the desired nanostructure), TiO_2 (anatase), NaCl, and NP-9 (nonylphenyl ether) were mixed (molar ratio 1:1:20:3), ground for 25 min, and finally sonicated for 5 min. The mixture was then placed in a quartz crucible, inserted into a quartz tube, annealed at 820 °C for 3.5 h, and subsequently cooled to room temperature. Samples were collected, washed several times with distilled water, and dried at 120 °C overnight in a drying oven. We could easily and routinely scale up this process to produce grams of single-crystalline $BaTiO_3$ and $SrTiO_3$ nanomaterials.

In fact, the molten salt synthesis (MSS) method described in the previous paragraph has been utilized as a simplistic methodology for producing ceramic oxide powders of varying morphologies and stoichiometries. Titanates, ferrites, niobates, and other perovskites represent a few examples of oxides that can be readily prepared by this process. Alterations in the amount and properties (*e.g.* anion size and solubility) of the salt utilized can have a profound effect on growth and reaction

environments with consequences for the resultant shape, morphology, and physicochemical characteristics of the particles formed.[2,62]

In our laboratory, we have used the MSS technique to prepare pristine $BaTiO_3$ nanowires with diameters ranging from 50 to 80 nm and an aspect ratio larger than 25 : 1, as well as single-crystalline $SrTiO_3$ nanocubes with a mean edge length of 80 nm (Fig. 4). As noted, we found it to be a simple, readily scaleable (in terms of grams) solid-state reaction in the presence of NaCl and a non-ionic surfactant. What determines the final shapes of these nanostructures may be the relative growth rates on the (100) *vs*. the (111) crystallographic planes, which in turn depends on the relative specific surface energies associated with the facets of the crystal. Although the fundamental basis of shape selectivity for this system is not as yet fully known, the preferential adsorption of molecules and ions in solution, such as chloride, to different crystal faces likely directs the growth of nanoparticles to their ultimate product morphology by controlling the growth rates along the different crystal faces.[19,63,64] Recent reports have demonstrated the importance of Cl^- ions, which are selectively adsorbed onto the (001) and (111) faces, in dramatically controlling the shape of copper nanocrystals.[64,65]

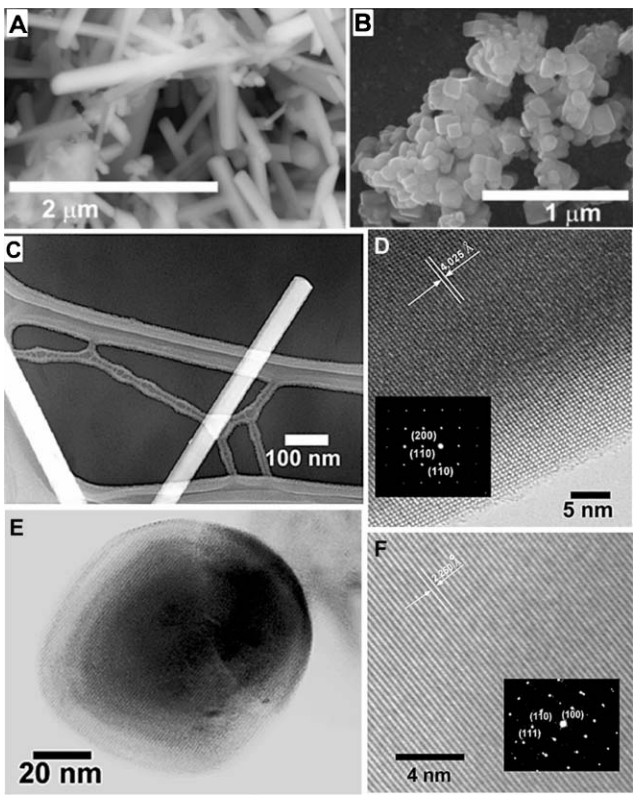

Fig. 4 SEM images of as-prepared (A) $BaTiO_3$ nanowires and (B) $SrTiO_3$ nanocubes. (C) Typical TEM micrograph of a $BaTiO_3$ nanowire. (D) HRTEM image of a portion of the nanowire in (C). Inset of (D) is the SAED pattern of a $BaTiO_3$ nanowire. (E) TEM micrograph of an individual $SrTiO_3$ nanocube. (F) HRTEM image of (E), showing the crystal lattices, corresponding to the cubic phase. Inset of (F) is the corresponding SAED pattern of the as-synthesized $SrTiO_3$ nanocubes. Reprinted with permission from reference 61. Copyright 2004 American Chemical Society.

Furthermore, this simple molten salt synthetic method recently has been extended to the preparation of a series of single-crystalline $Ca_{1-x}Sr_xTiO_3$ ($0 \leqslant x \leqslant 1$) nanoparticles (Fig. 5).[66–69] The composition of the resulting nanoparticles is reproducibly tunable by adjusting the ratio of the reactants. Shapes of the generated $Ca_{1-x}Sr_xTiO_3$ nanoparticles alter from cubes to quasi-spheres with decreasing 'x' values. Typical nanoparticles have sizes ranging between 70 and 110 nm, irrespective of the Sr or Ca content. Our powder X-ray diffraction (XRD) results from these $Ca_{1-x}Sr_xTiO_3$ ($0 \leqslant x \leqslant 1$) nanoparticles are consistent with the sequence of phase transitions with increasing Sr content in the $Ca_{1-x}Sr_xTiO_3$ system as progressing from orthorhombic (*Pbnm*) to orthorhombic (*Bmmb*) followed by tetragonal (*I*4/*mcm*) and ultimately to cubic (*Pm*3*m*) when $x = 1$, as previously observed for the bulk.[70] Although this phase transition sequence still requires further study to confirm its validity, the implications of this result are that the physical properties of $Ca_{1-x}Sr_xTiO_3$ nanoparticles can be controllably modified by adjusting the composition. As an example of the significance of this synthetic capability, the availability of nanosized $Ca_{0.7}Sr_{0.3}TiO_3$ particles may enhance the material's existing usage as an efficient dielectric barrier for the plasma-induced, catalyst-free decomposition of CO_2.[71]

3. Nanostructures of titania and of alkali metal titanates

3.1. Introduction

Titanium oxide (titania: TiO_2) is a wide band gap material (3.0–3.2 eV), which exists in three main crystalline phases: anatase, rutile, and brookite. These materials have been utilized as components of applications including but not limited to batteries, photovoltaic cells, advanced photocatalysts for environmental purification, pigments, cosmetics, photonics, optoelectronic devices, and gas sensors, partly due to their low cost, chemical stability, and robustness under UV illumination.[72–75] Titania nanotubes, nanowires, and nanoparticles are particularly interesting, because their catalytic activity is dependent on particle size, surface area, and porosity.[76]

Titania does not intrinsically exhibit a lamellar feature, since the strong ionic interactions keep the metal cations and oxygen anions together. As such, the observation of layered walls in titania nanotubes has been a source of controversy, especially since there have been reports that the nanotubes may actually consist of lepidocrocite-type protonic titanates.[77,78]

Alkali metal titanates have the general formula of $A_2Ti_nO_{2n+1}$ or $A_2O{\cdot}nTiO_2$ (A = alkali metal ion or proton, n = 1–9) and display a number of interesting catalytic, conductive, and intercalation properties depending on the value of 'n'. Apart from being chemically stable, what is interesting about titanates is that because they are analogous to charged polyelectrolytes, they can be delaminated to form exfoliated nanosheets, which are useful as building blocks for new materials. For instance, nanocomposites of inorganic layered hosts with bulky guests have been prepared by assembling nanosheets in their presence. These guest systems

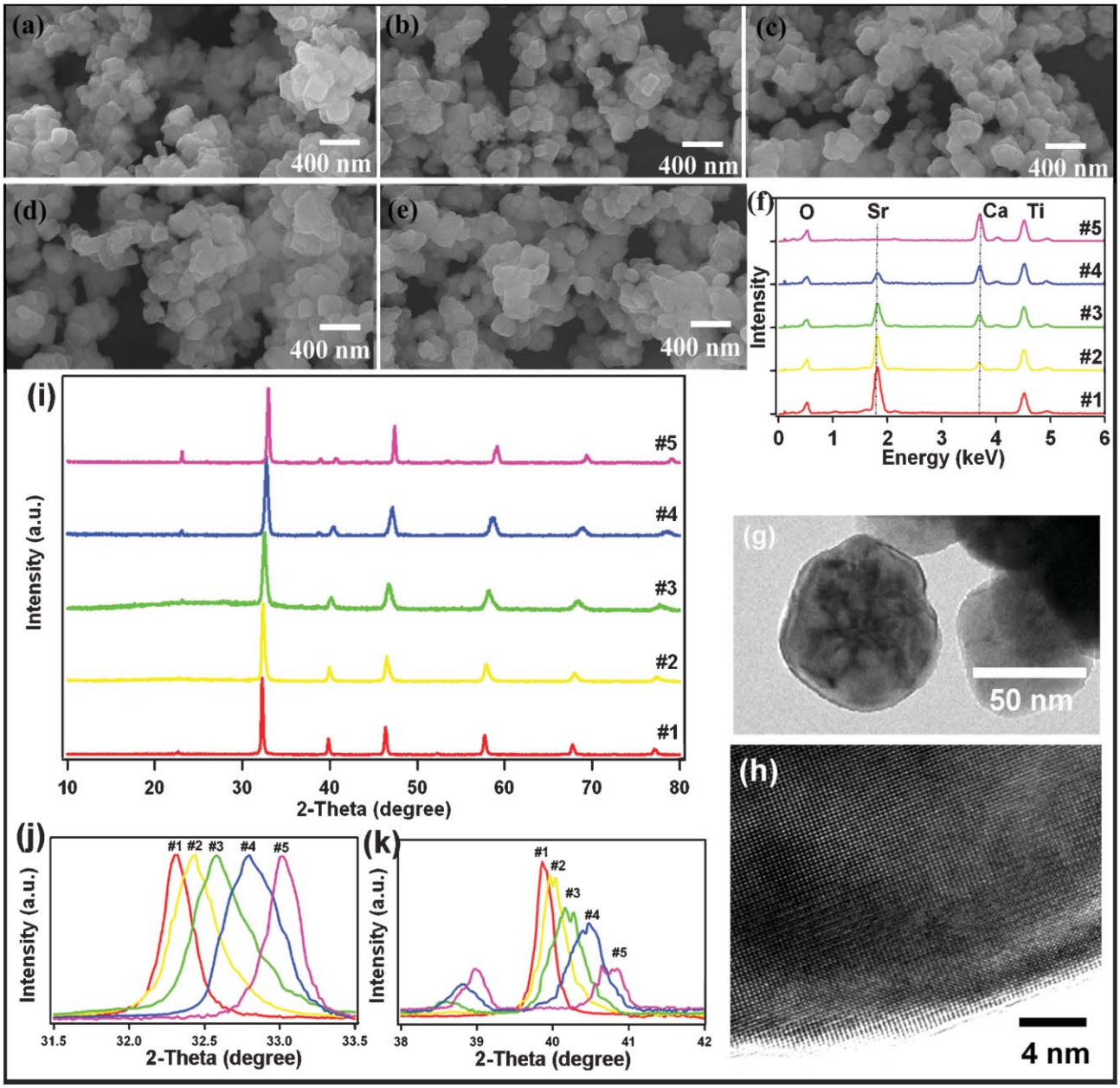

Fig. 5 SEM images of as-prepared $Ca_{1-x}Sr_xTiO_3$ nanoparticle samples: (a) $SrTiO_3$, (b) $Ca_{0.3}Sr_{0.7}TiO_3$, (c) $Ca_{0.5}Sr_{0.5}TiO_3$, (d) $Ca_{0.7}Sr_{0.3}TiO_3$, and (e) $CaTiO_3$. (f) Energy-dispersive X-ray spectroscopy (EDS) data of the as-synthesized $Ca_{1-x}Sr_xTiO_3$ nanoparticles. (#1) $SrTiO_3$, (#2) $Ca_{0.3}Sr_{0.7}TiO_3$, (#3) $Ca_{0.5}Sr_{0.5}TiO_3$, (#4) $Ca_{0.7}Sr_{0.3}TiO_3$, and (#5) $CaTiO_3$. Labels are identical for (i), (j), and (k). The intensity of the peaks for each sample has been normalized based on the intensity of the Ti peak. (g) A typical TEM image of the as-prepared $Ca_{0.5}Sr_{0.5}TiO_3$ nanoparticle sample. (h) HRTEM image of a $Ca_{0.5}Sr_{0.5}TiO_3$ nanoparticle. (i) XRD patterns of as-prepared $Ca_{1-x}Sr_xTiO_3$ nanoparticle samples in the 2θ range of 10 to 80°. (j) The 2θ diffraction peak around 32.5° for the samples of all five compositions. These illustrate a gradual increase in lattice parameter observed as a function of increasing calcium concentration in $Ca_{1-x}Sr_xTiO_3$ nanoparticles. (k) The 2θ diffraction peaks centered at 40° for the samples of all five compositions, showing the phases of as-prepared $Ca_{1-x}Sr_xTiO_3$ nanoparticles varying from cubic to tetragonal to orthorhombic with decreasing 'x' content. Reprinted with permission from reference 69. Reproduced with permission of Wiley-VCH.

have ranged from organic polymers, polyoxocations to biocatalytic hemoglobin.[79,80] Moreover, layer-by-layer manipulation and other self-assembly techniques have been used to construct thin films and other more complicated functional assemblies.[81–83] In particular, trititanate nanotubes are of significant fundamental interest because one-dimensional channels and interlayer spaces coexist in these systems.[84,85] An example is the H-form of trititanate, $H_2Ti_3O_7$, a potential proton-conducting fuel cell electrolyte.[86] Alkali metal titanates have become important for their exciting photocatalytic capabilities (including their ability to photocleave water) and their ion-exchange/intercalation properties.[87–89] As a result of the wide range of valued functional properties in these materials, it is important to rationally control the size, morphology, and assembly of titania and titanate nanostructures.

3.2. Synthetic approaches to 1-D nanostructures

Indeed, a number of syntheses of 1-D nanostructures of titanates and titanium dioxide and their related two-dimensional (2-D) arrays have been achieved in recent years. The main preparative methods can be broadly divided into four approaches. The first involves the template method in which tubulous TiO_2 nanostructures have been made by using alumina, polycarbonate, or organogel templates combined with a sol-gel polymerization in the presence of an aqueous solution system of titanium tetrafluoride or titanium isopropoxide.[90–94] The second is associated with an anodic oxidation method, wherein TiO_2 nanotubes are fabricated by anodic oxidation of a pure titanium foil in an aqueous solution containing 0.5 to 3.5 wt% hydrofluoric acid with a platinum counter electrode at anodization voltages ranging from 10 to 20 V for up to 45 min.[74] The third is related to electrospinning. For instance, long, hollow nanofibers with uniform circular cross-sections and with walls made of inorganic–polymer composites can be prepared by the electrospinning of two immiscible, precursor liquids through a coaxial, two-capillary spinneret followed by selective removal of the cores.[95] The last and most controversial method is associated with a hydrothermal treatment, in the presence of concentrated NaOH, of either (i) TiO_2 in either bulk, powder, or nanoparticle form or (ii) a $TiOSO_4 \cdot H_2O$ solution at temperatures in the range of 100 to 160 °C, which tends to produce layered titanate nanostructures (Fig. 6).[77,78,84,85,96–102]

The hydrothermal synthetic approach merits a more detailed discussion. It was initially proposed by Kasuga *et al.*[96] that hydrothermal recrystallization of TiO_2 particles in concentrated aqueous NaOH solution could routinely produce high purity anatase TiO_2 nanotubes. In effect, it was concluded that washing the alkali-treated sample with water and further reaction with HCl were the two crucial steps in the formation of these types of nanotubes. This was a highly interesting result for a very important reason. While this technique tended to be more applicable to the generation of morphologies of layered structures such as C, $B_xC_yN_z$, MS_2 (M = Mo, W, Nb, Ta), $NiCl_2$, vanadium oxide, InS, and Bi nanotubes, many important non-layered metal oxides such as TiO_2, MnO_2, ZrO_2, and Nb_2O_5 have generally required the use of templates (*e.g.* carbon nanotubes or anodic alumina oxide) to provide for spatial confinement of the as-generated nanostructures. Hence, controversy arose as to the exact physical and chemical composition of these TiO_2 nanomaterials.

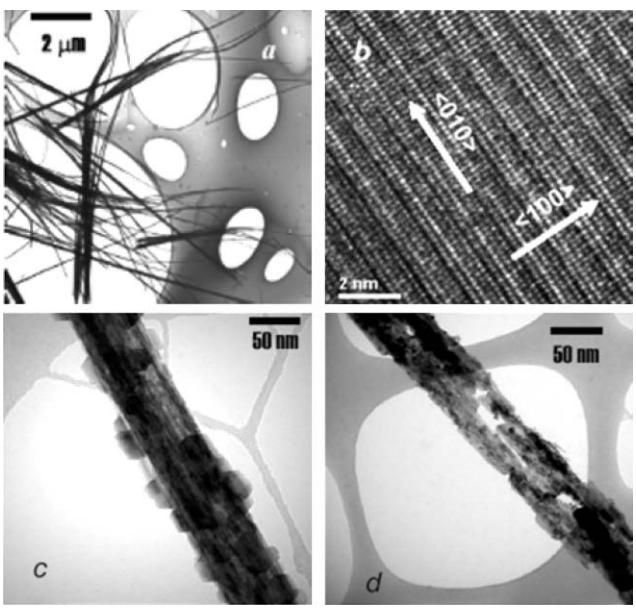

Fig. 6 TEM images of the samples. (a) H-titanate fibers, (b) HRTEM image of the fibers, (c) the product of the phase conversion reaction at 373 K, a titanate fiber covered with anatase crystals, and (d) the product obtained at 393 K, fibril aggregates of anatase nanocrystals. Reprinted with permission from reference 101. Copyright 2004 American Chemical Society.

For instance, based on XRD and high-resolution transmission electron microscopy (HRTEM), Chen *et al.*[84,85] proposed that the product, synthesized by Kasuga *et al.*,[96] was actually not titania but rather consisted of rolled up individual layers derived from a $H_2Ti_3O_7$ structure with a C-centered monoclinic unit cell with $a = 1.603$, $b = 0.375$, $c = 0.919$ nm, and $\beta = 101.45°$. However, the presence of protons in the interlayer space could not be detected by HRTEM in their work. Thorne *et al.*[103] suggested that the stoichiometry of the material was $H_2Ti_3O_7 \cdot 0.8H_2O_{abs}$ on the basis of thermal analysis, and confirmed the presence of structural protons and of trapped water molecules by solid-state nuclear magnetic resonance (NMR) spectroscopy. Ma *et al.*[81,104] studied the structural characteristics of high-purity nanotubes and nanobelts, controllably obtained in hydrothermal treatments, of varying temperature and duration, of anatase TiO_2 in concentrated NaOH solution. By employing XRD, Raman, X-ray absorption fine structure, and electron diffraction analyses, their results revealed that these nanotubes and nanobelts may actually be comprised of a layered titanate structure, more specifically pertaining to an orthorhombic lepidocrocite titanate nanotube model. Similarities and differences amongst the various nanotubes/nanobelts and other bulk titanates, represented by trititanate $H_2Ti_3O_7$ and lepidocrocite-type $H_{0.7}Ti_{1.825}\square_{0.175}O_{4.0} \cdot H_2O$, were also described.

3.3. Three-dimensional nanostructures

One way of further assembling a wide range of these titania and titanate nanostructures is using the bottom-up approach. Many applications involving TiO_2 and titanate require their organization into three-dimensional (3-D) structures, especially as monodisperse colloids, which are technologically significant in a broad range of applications, including but not limited to drug delivery vehicles, fillers, sensors, catalysts, and photonics.[105] Whereas, to date, there has not been a published report on generating 3-D assemblies of titanate nanostructures, four sets of approaches have been developed to generate micron as well as submicron-sized structures of TiO_2. The first technique generates monodispersed spherical colloids of titania by using a modified sol-gel method with glycolated precursors.[106] A second process produces hollow titania spheres from a layered precursor deposition on sacrificial colloidal core particles.[107] A third procedure involves the use of an ionic liquid-based synthesis of hollow TiO_2 microspheres in a

single-step reaction.[108] A fourth method uses a simple 'one-pot' reaction to prepare hollow anatase nanospheres *via* Ostwald ripening under hydrothermal conditions.[109] Nevertheless, none of this prior work can truly create organized self-assemblies with particular, long-range functionality in any timely fashion.

In our laboratory, we have developed a general synthetic strategy aimed at the preparation of ordered structural motifs of anisotropic titanate and TiO_2 structures at the mesoscopic level. Briefly, we have adapted a template-free hydrothermal reaction to produce titanate precursors and followed that protocol with an *in situ* chemical transformation to synthesize anatase titania (Fig. 7). Essentially, our work describes the preparation of 3-D dendritic assemblies of individual titanate and titania 1-D nanostructures; these 1-D nanostructures individually measure several hundreds of nanometers in length and up to several nanometers in diameter. These hierarchical structures have been produced using a general redox strategy combined with a hydrothermal reaction involving a titanium source (*e.g.* either Ti foil or Ti powder), a basic NaOH or KOH solution, and an oxidizing H_2O_2 solution. Whereas a similar study was limited exclusively to the formation of titania nanorods on a Ti plate surface,[110] by contrast, we have been

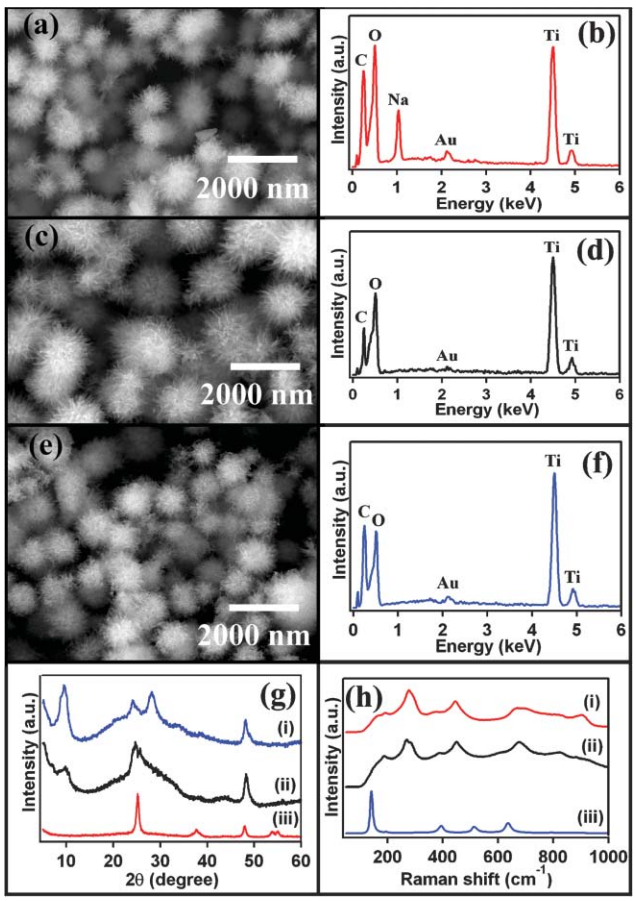

Fig. 7 Typical SEM micrographs and EDS data of as-prepared powders of 3-D dendritic nanostructures of nanowires. (a & b) sodium hydrogen titanate; (c & d) hydrogen titanate; and (e & f) TiO_2. (g) and (h) are the XRD patterns and Raman spectra of: (i) sodium hydrogen titanate, (ii) hydrogen titanate, and (iii) TiO_2, respectively.

able to readily generate large quantities of discrete urchin-like structures not only of both titanate and titania 1-D nanostructures but also in different reaction media simultaneously, including in solution and on the surfaces of our Ti reagent foils and powders. Put another way, we have for the first time generated 3-D dendritic assemblies of (a) potassium hydrogen titanate, (b) sodium hydrogen titanate, (c) hydrogen titanate, and (d) anatase titania in solution and on surfaces.

Typically, as-prepared 3-D assemblies of titanate and titania 1-D nanostructures have overall diameters ranging from 0.8 μm to 1.2 μm, while the interior of the aggregates are hollow with a diameter range of 100 to 200 nm, resembling the microscopic variant of a sea urchin with spines. The component, constituent titanate and anatase titania 1-D nanostructures have a diameter range of 7 ± 2 nm and possess lengths of up to several hundred nm. SEM and TEM results provide for strong, corroborating evidence that the progression of the chemical reaction from titanate to anatase titania has little if any impact on the actual physical dimensions of either the 1-D or 3-D structural motifs. Microscopy data also showed that the constituent 1-D nanostructures are single-crystalline in nature with the presence of surface amorphous layers. Although these titania and titanate 1D nanostructures appear to be loosely attached to each other, we found that brief sonication for up to one hour could not visibly disrupt the 3-D assemblies, implying that interactions amongst the constituent 1-D nanostructures were particularly strong.

We have even been able to conveniently section these 3-D structures and have developed insights into their formation mechanism. In effect, crystalline supramolecular assemblies may arise either from the intrinsic packing characteristics of molecules or from the interplay of subtle interactions involving external energy and mass transport considerations.[111] In our experiment, to investigate the growth mechanism of hollow micron-scale spheres of titanate 1-D nanostructures, the corresponding time-dependent evolution of 3-D hierarchical crystal morphology and of the surface roughness of the foil were recorded by scanning electron microscopy (SEM) and atomic force microscopy (AFM), respectively, over a reaction course of 6 hours. The temporal evolution of titanium concentration in a 3 ml reaction solution was also monitored by inductively coupled plasma atomic emission spectrometry (ICP-AES) over the identical time period. It is plausible to postulate that our cumulative observations are the result of a two-stage mechanism involving the initial formation of primary 1-D nanostructures that subsequently self-assemble, or more specifically, a "growth-then-assembly" process.[112,113] That is, the primary 1-D nanostructures of alkali metal hydrogen titanates (such as sodium hydrogen titanates) form initially from the hydrothermally driven direct rolling up of 2-D nanosheets generated *in situ* on the Ti foil surface due to the redox reaction of Ti with H_2O_2 in the presence of alkali metal hydroxide (such as NaOH solution).[81,114] These 1-D nanostructures of titanates subsequently assemble into spherical 3-D dendritic aggregates.[81,114,115]

Moreover, subsequent acid leaching and neutralization exchange the Na^+ with H^+ to form the assemblies of hydrogen titanate 1-D nanostructures.[77] Our Raman, XRD, and HRTEM results also support the notion that the assemblies

of these layered titanates have an orthorhombic lepidocrocite-type $H_{0.7}Ti_{1.825}\square_{0.175}O_{4.0}\cdot H_2O$ structure. A high-temperature annealing treatment in air at 350 to 500 °C for 1–10 h and accompanying dehydration process transform these assemblies of titanate 1-D nanostructures into their anatase TiO_2 analogues without atom-by-atom recrystallization of anatase.[101]

The template-free synthesis of discrete hierarchical structures of 1-D nanostructures reported by our group is a simple, inexpensive, scalable, and mild synthetic process. We have also demonstrated that the micron scale assemblies of TiO_2 1-D nanostructures are active photocatalysts for the degradation of synthetic Procion Red dye under UV light illumination. Thus, the high quality micron scale, urchin-like structures synthesized can be expected to be incorporated as functional components of photonic devices, dye-sensitized solar cells, as well as photocatalysts.

4. Nanostructures of bismuth ferrites

4.1. Introduction

Multiferroics are simultaneously ferroelectric, ferromagnetic, and ferroelastic.[6,31,116–118] These materials possess a spontaneous polarization, magnetization, and piezoelectricity that can be switched on by an applied electric field, magnetic field, and elastic force or stress, respectively. The investigations of their fundamental physical properties suggest that these materials can be used for information storage, quantum computing, spintronics, sensors, and multiple-state memory media.[116,119] Prototypical examples of existing multiferroics maintain the perovskite structure and include $RMnO_3$ (with R = Sc, Y, In, Bi, Ho, Er, Tm, Yb, Lu) as well as $BiFeO_3$.[120] The general class of bismuth ferrites, including $BiFeO_3$, $Bi_2Fe_4O_9$, and $Bi_4Fe_2O_9$, consists of semiconductors possessing interesting properties which are significant for applications in various fields including optics, electronics, magnetism, information processing and storage. Stimulated by the scientific potential and applications of these materials, there have been considerable efforts, expended in synthesizing bismuth ferrite nanostructures. In this section, we focus explicitly on the production of $BiFeO_3$ and $Bi_2Fe_4O_9$ nanostructures.

4.2. $BiFeO_3$

$BiFeO_3$ shows ferroelectricity with a high Curie temperature (T_C) of ~1103 K, and antiferromagnetic or weak ferromagnetic properties below a Neél temperature (T_N) of 643 K.[121] In its bulk form, measurement of ferroelectric and transport properties in bismuth ferrite has been limited by leakage problems, likely due to low resistivity, defect, and non-stoichiometry issues. To address this problem, recent approaches have focused on developing novel structures of $BiFeO_3$.[121–124]

For instance, $BiFeO_3$ nanoparticles, with average sizes of 21 to 59 nm, were prepared from precursor materials including Bi_2O_3, $Fe(NO_3)_3\cdot 9H_2O$, citric acid, and a dispersion agent in diluted nitric acid.[122] Preliminary magnetic property measurements of these nanoparticles were performed, showing enhanced properties corresponding to reduction of size, an effect discussed on the basis of Mössbauer results. Very recently, the preparation of nanosized bismuth ferrites from $Bi(NO_3)_3$ and $Fe(NO_3)_3$ precursors with tartaric acid in nitric acid was reported; particle sizes obtained were in the range of 3 to 16 nm.[124]

In our group, systematic studies on $BiFeO_3$ nanoparticles prepared by a modified sol-gel method have been performed.[125] As-prepared $BiFeO_3$ nanostructures turned out to be a series of single-crystalline nanoparticles with mean sizes of ~20 to 100 nm, respectively. The magnetic properties of as-prepared $BiFeO_3$ nanostructures were also investigated based on Mössbauer as well as SQUID (superconducting quantum interference device) measurements; strong correlations of these data with the sizes of the sample were observed. In addition, optical characterization of these $BiFeO_3$ nanostructures was performed using Raman, UV-visible, and IR spectroscopies.

To our knowledge, there have not been any viable syntheses of 1-D nanostructures of $BiFeO_3$ reported. The fabrication of 1-D nanostructures of $BiFeO_3$ is of fundamental importance in investigating size correlation of the basic physical properties of these materials with implications for their device applications. In our recent work,[123] we have employed a pressure-filter variation of a template synthesis involving the sol-gel technique[126,127] for the synthesis of $BiFeO_3$ nanotubes (NTs), because of its practicality,[128,129] its relative simplicity, and its prior versatility in the preparation of high aspect ratio nanostructures of ternary metal oxides.[21,48] A schematic of the procedure is shown in Fig. 8. As-prepared $BiFeO_3$ 1-D nanotubes were subsequently characterized by a number of techniques, including XRD, SEM, TEM, as well as EDS and SAED. Microscopy analysis showed that as-prepared $BiFeO_3$ NTs, derived from porous alumina membranes having pore sizes of 200 nm, had straight and smooth structures, and that their outer diameters were in range of 240 to 300 nm with lengths ranging from several microns to as much as 50 microns. The aspect ratio for the tubes could attain values as high as 200 : 1. $BiFeO_3$ NTs having outer diameters in the range of 140 to 180 nm and lengths of up to several microns, were prepared from 100 nm pore-sized templates; these structures consisted of straight tubes though their surfaces were relatively rough and irregular. The difference in morphologies of the tubes synthesized in 100 *vs.* 200 nm pore-sized templates could have

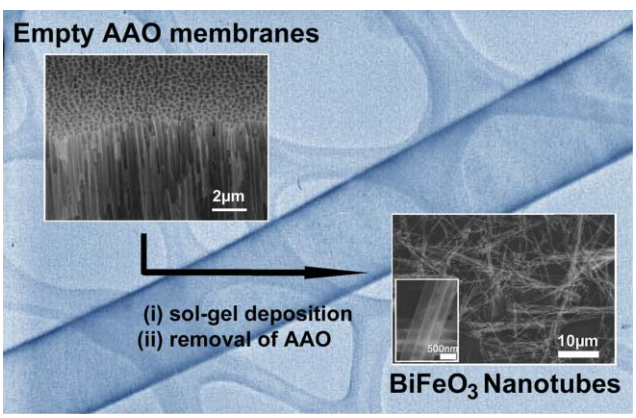

Fig. 8 A schematic of the fabrication of $BiFeO_3$ nanotubes using a template methodology, which is superimposed upon a TEM image of the resultant product tube. Reprinted with permission from reference 123. Copyright 2004 Royal Society of Chemistry.

arisen not only from differential chemical interactions of the various sol constituents with the pore walls themselves but also from contrasting geometric configurations of the sol constituent molecules within each individual template membrane, induced by spatial constraints. Moreover, as the nucleation of the $BiFeO_3$ particles likely starts from sites randomly located on the wall of the template, the net effect would be formation of polycrystalline $BiFeO_3$ NTs, consistent with the SAED and HRTEM results observed. Preliminary magnetic property measurements, performed using a SQUID, showed a small though appreciable level of magnetization, unlike that for pure bulk $BiFeO_3$.

Among the classes of $BiFeO_3$ nanostructures, 2-D nanostructures of $BiFeO_3$, *e.g.*, thin films or nanofilms, have been extensively studied, as compared with 0-D or 1-D nanostructures. For instance, thin films of $BiFeO_3$ (with a thickness range of 50 to 500 nm) show enhanced physical properties relative to that of the bulk.[121] Phase-pure $BiFeO_3$ thin films, having thickness values of 50 to 500 nm, were successfully grown using pulsed laser deposition (PLD) onto single crystal $SrTiO_3$ substrates[130,131] as well as onto Si[132] and $Pt/TiO_2/SiO_2/Si$[133] substrates. Different synthetic approaches, such as the use of liquid phase epitaxy (LPE) and sol-gel methods onto $SrTiO_3$ and $LaAlO_3$ substrates, as well as the utilization of chemical solution deposition and spin-coating techniques onto (111) $Pt/Ti/SiO_2/Si$ substrates have also been employed to fabricate thin films of $BiFeO_3$.[134–137] In addition to these recent synthetic efforts, a first-principles study of multiferroic $BiFeO_3$ has been performed in order to further understand its intrinsic physical properties such as spontaneous polarization.[138]

4.3. $Bi_2Fe_4O_9$

Because of their high sensitivity to ethanol and acetone vapors, bismuth ferrites have been recently considered as new materials for semiconductor gas sensors.[139,140] In particular, the catalytic potential of $Bi_2Fe_4O_9$ for ammonia oxidation to NO is of current interest as these iron-based materials may likely replace current, irrecoverable, and costly catalysts based on platinum, rhodium, and palladium.[141,142] Despite the evident importance of $Bi_2Fe_4O_9$ as a functional material, very few reports have appeared associated with nanoscale structural motifs of this bismuth ferrite.[142,143] Sheet-like nanoparticulate powders have been formed using a hydrothermal technique.[142] In that study, factors such as the role of the concentration of the metal ions, alkalinity in the precursor solution, and temperature were examined and were claimed to be more important determinants of $Bi_2Fe_4O_9$ nanoparticulate formation than that of the molar ratio of Bi^{3+} to Fe^{3+} precursors.

Our group has reported on the fabrication of discrete single-crystalline submicron-sized $Bi_2Fe_4O_9$ cubic structures as well as their elongation into orthorhombic and rod-like structures (Fig. 9).[144] In this work, a molten salt technique was employed, due to the intrinsic simplicity, non-toxicity, facility of use, and versatility in the preparation of single-crystalline metal oxides. The roles of surfactant, salt, precursor identity, as well as alterations in the molar ratio of Bi^{3+} to Fe^{3+} precursors were systematically examined and correlated with the predictive formation of different shapes of $Bi_2Fe_4O_9$ products. For example our observations confirmed that there is an only very narrow combination of experimental parameters such as (a) a 1:1 molar ratio of precursors, (b) the addition of salt, (c) the presence of surfactant, and (d) the usage of specific elemental precursors, that collectively will yield single-crystalline $Bi_2Fe_4O_9$ cubes with predictive control of shape and size. The presence of salt is expected to decrease the melt viscosity and thereby increase the mobility of components within the molten flux, whereas the presence of surfactant may prevent interparticle aggregation by forming a 'shell' around individual particles.[145]

Extensive structural characterization of as-prepared cubic $Bi_2Fe_4O_9$ products was performed and representative SEM images of the cubes are shown in Fig. 9. A typical mean edge length of the cubes obtained was 386 ± 147 nm, and the faces were essentially flat. In addition to structural characterization of $Bi_2Fe_4O_9$ cubes using microscopic means, Mössbauer and SQUID measurements were also performed and the results showed a slightly lower T_N of the cubes (250 K) as compared with that of the bulk (263 K).

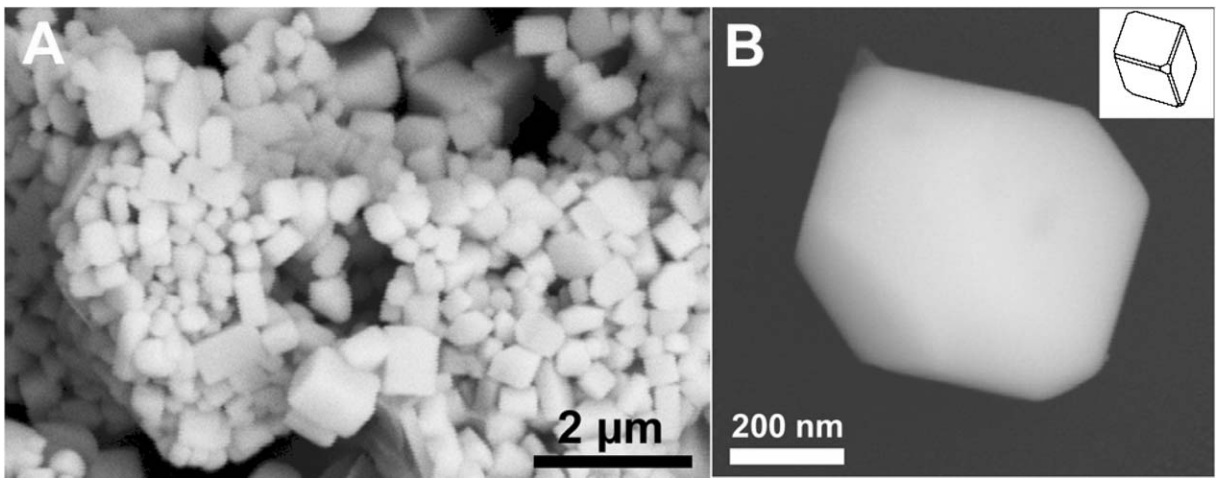

Fig. 9 SEM images of (A) $Bi_2Fe_4O_9$ cubes and (B) a typical individual $Bi_2Fe_4O_9$ cube, prepared using a molten salt method. The inset of (B) illustrates a schematic of the facets of an individual cube. Reprinted with permission from reference 144. Copyright of 2005 Royal Society of Chemistry.

5. Nanostructures of ABO_4-type materials

5.1. Introduction

The ABO_4 class of oxides, wherein A and B consist of two different elements with oxidation states of +2 and +6, respectively, are a family of inorganic materials with potential in various applications, such as photoluminescence, microwave applications, optical fibers, scintillator materials, humidity sensors, magnetic properties, and catalysis. For example, 'A' not only can be an alkaline earth metal but also can be identified with (but not limited to) Pb, Zn, Cd, Fe, Mn, Co, or Ni. On the other hand, 'B' can be associated with elements including (but not limited to) W, Mo, Cr, I, Se, or S.[146,147]

In our laboratory, we have chosen to focus on the fabrication of nanorods of $BaWO_4$ and $BaCrO_4$, which are compositionally and structurally representative of the ABO_4 class of metal oxides.[146,147] Barium tungstate or barite is important in the electro-optical industry due to its emission of blue luminescence. In addition, its interesting thermoluminescence and stimulated Raman scattering (SRS) properties render barium tungstate as a candidate for the design of solid-state lasers that can emit radiation within a specific spectral region. As such, these materials are of use for medical laser treatment applications, up-conversion fiber lasers, and analogous spectroscopic functions.[148–150] Barium chromate is a naturally occurring chromate analogue of barite. It has often been used as an oxidizing agent and as a catalyst for enhancing vapor-phase oxidation reactions.[151] Moreover, due to its excellent photophysical properties, barium chromate is a highly efficient photocatalyst, with a particularly marked response to visible light irradiation.[152]

5.2. Synthetic approaches

Recently, remarkable progress has been achieved regarding the preparation of low-dimensional nanoscale metal tungstate, chromate, and sulfate derivatives. The synthesis of ordered microarrays of nanocrystals of both barium chromate and sulfate, with controlled chemical composition and size distribution, was reported using a reversed micelle templating method.[153] This methodology was subsequently extended to generate barium tungstate nanorods; the 2-D organization of these $BaWO_4$ and $BaCrO_4$ nanorods at the water–air interface was accomplished using a Langmuir–Blodgett technique.[154,155] Recently, high aspect-ratio, single-crystalline $BaWO_4$ and $BaCrO_4$ nanowires with diameters as small as 3.5 nm and lengths up to more than 50 microns were synthesized in catanionic reverse micelles formed by an equimolar mixture of two surfactants: undecylic acid and decylamine.[156,157] With the further use of double-hydrophilic block copolymers as effective crystal growth modifiers, morphological variants, namely penniform $BaWO_4$ nanostructures, could be prepared using this technique (Fig. 10).[158] Using an analogous idea, different $BaCrO_4$ nanostructures have been processed through a polymer-directed synthesis.[146,159–161] However, the development of facile, mild, and effective approaches for creating size-controlled 1-D nanostructures and their associated novel architectures has remained a significant scientific challenge. Finally, uniform tungstate nanorods/nanowires[146] such as

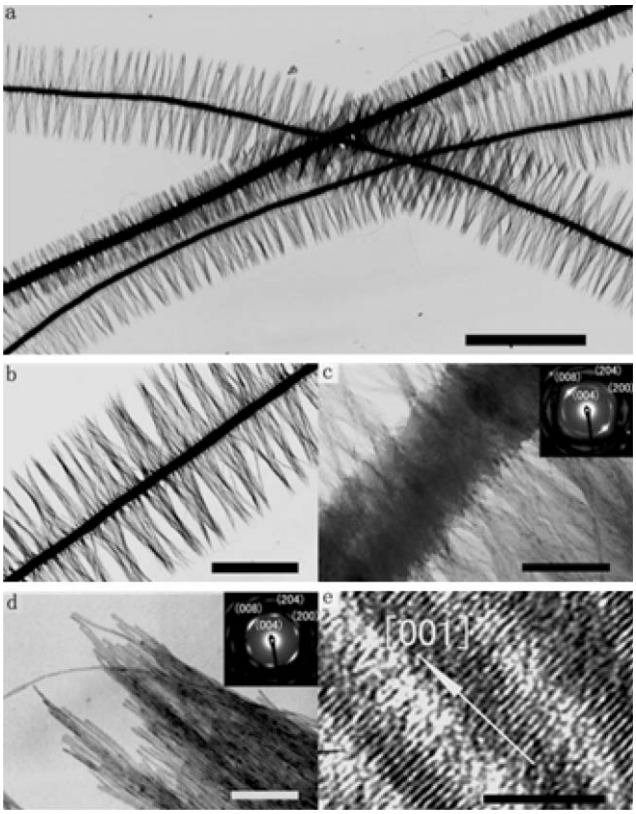

Fig. 10 TEM (a–d) and HRTEM (e) images of penniform $BaWO_4$ nanostructures obtained in the presence of 0.5 g L^{-1} PEG-*b*-PMAA after aging for 8 h. Insets show the corresponding electron diffraction patterns. Scale bars: (a) 5 μm, (b) 2 μm, (c) 200 nm, (d) 100 nm, and (e) 5 nm. Reprinted with permission from reference 158. Copyright 2003 American Chemical Society.

MWO_4 (M = Zn, Mn, Fe) with diameters of 20–40 nm and lengths of up to micrometers were prepared by hydrothermal transformation and recrystallization of amorphous particulates under mild conditions without the use of special ligands or surfactants. A variation of this technique could produce $BaWO_4$ crystals of different morphologies ranging from olive-like to flake-like to whisker-like structures in the presence of different surfactants.[162]

5.3. A general, room-temperature method for the synthesis of isolated as well as arrays of single-crystalline ABO_4-type nanorods

Our recent work demonstrates a room-temperature preparation, using a novel, modified template-assisted methodology, of straight, smooth, single-crystalline $BaWO_4$ nanorods and $BaCrO_4$ nanorods with controllable sizes as well as the creation of arrays of these nanorods in the pores of an alumina membrane (Fig. 11).[163] For example, diameters of $BaWO_4$ nanorods were ~200 $\pm$ 25 nm with lengths attaining several microns, based on the 200 nm pore sizes of the alumina membranes used in the synthesis. By analogy, based upon the 100 nm pore size of the alumina templates utilized, the corresponding diameters of $BaCrO_4$ nanorods fabricated were in the range of 100 $\pm$ 15 nm, with aspect ratios of up to 15 : 1. The resulting nanorods and their associated arrays have been

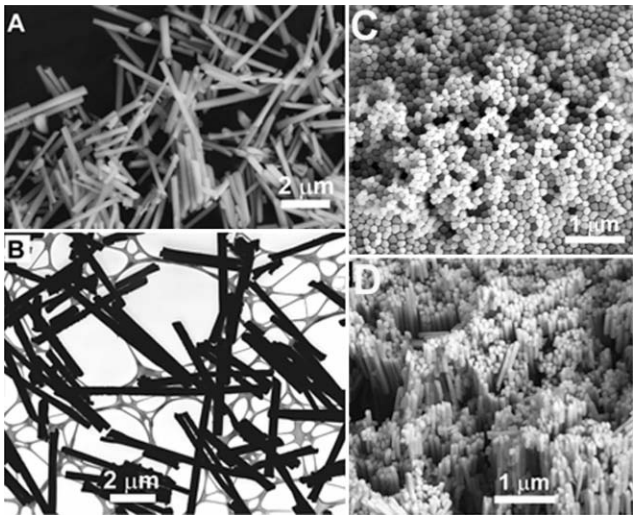

Fig. 11 (A) Typical SEM micrograph of $BaWO_4$ nanorods. (B) Representative TEM image of $BaWO_4$ nanorods and SEM images of as-prepared $BaWO_4$ nanorod arrays: (C) top-view and (D) tilt-view. Reprinted with permission from reference 163. Copyright 2004 American Chemical Society.

extensively characterized using a variety of microscopy, spectroscopy, and diffraction results.

Specifically, a modified template synthesis technique, originally developed for the synthesis of organic microtubules, was used to successfully prepare free-standing single-crystalline $BaWO_4$ and $BaCrO_4$ nanorods and their arrays by physically placing two different precursor solutions in two halves of a U-tube cell, respectively, separated by alumina template membranes. In other words, the pores in alumina membranes were used as the confining environment in which to control the growth of well-defined morphologies of our ABO_4 nanostructures. The membranes used are thin, and are mounted in a double-diffusion setup, which enables the continuous flow of ions into the membrane pores and thus, the production of nanoscale single crystalline ABO_4-type materials. The shape of the alumina membranes has a dramatic effect on the morphology of the ABO_4 phase that subsequently forms. In fact, we note instances where the morphology of the ABO_4 nanorods spatially maps out the interior nanoscopic profile and localized contours of the internal pores of the alumina membranes. That is, whereas the majority of as-prepared $BaWO_4$ and $BaCrO_4$ nanorods were straight and possessed smooth surfaces, a small number of $BaWO_4$ and $BaCrO_4$ nanorods with protrusions or depressions on their surfaces were also produced, accurately reflecting the morphology and inner surface roughness of the pores from whence they were formed.

What is significant is that most nanostructures previously produced by conventional templating procedures are polycrystalline,[12] in spite of the variety of different deposition strategies used, including electrochemical deposition, electroless deposition, polymerization, sol-gel deposition, and layer-by-layer deposition in nanoporous templates, because many of these prior methodologies require additional annealing steps at high temperature.[5,6,51,91] By contrast, the formation mechanism of nanorods under our experimental conditions is analogous to a biomimetic crystallization process.[164] That is, the growth of our nanorods within the confinement of alumina membranes is analogous to the precipitation of single crystals of calcium carbonate and calcium phosphate within the confinement offered by gels, micelles, chitin scaffolds, and collagen matrixes.[165–167] Hence, nucleation and growth of single-crystalline nanomaterials occur essentially instantaneously through the direct chemical interaction between ions of the two different precursor solutions diffusing towards and eventually reacting with each other. The membrane acts to spatially direct and confine crystal growth.

Moreover, at the same time, our simplistic technique allows for the reproducible fabrication of ordered, monodisperse 3-D arrays of these 1-D nanomaterials. This is critical, because assembly of nanoscale components is a key step toward building functional devices,[24] important for applications including nanoscale electronics and molecular sensing. Specifically, the fabrication of thermally stable 3-D arrays of 1-D nanomaterials, such as nanorods, is useful for optoelectronic applications, such as room-temperature ultraviolet lasing.[168] Though a number of fabrication methodologies have been reported for generating these types of nanoscale architectures,[97,169–171] none of these techniques appears to work for ABO_4-type compound systems, with the exception of the current work. Furthermore, although we have primarily focused on isolated 100 and 200 nm-sized $BaWO_4$ and $BaCrO_4$ nanorods and their associated arrays, we have noted that we can reproducibly form different sizes of these various nanoscale architectures using alumina template membranes of varying pore sizes. Because of the simplicity and generalizability of the approach used, it is anticipated, as earlier implied, that this methodology can be generalized to the synthesis of other important tungstate, molybdate, chromate, sulfate, iodate, and selenate systems as well as their complexes at the nanoscale. Moreover, we can prepare smaller-diameter single-crystalline nanorods using smaller-sized templates.

6. Nanostructures of other classes of ternary oxide materials

Mixed valence manganites of formula $R_{1-x}A_xMnO_3$, where R is a rare earth element and A is divalent Ca, Sr, or Ba, exhibit colossal magnetoresistivity.[172–174] In these systems, the interplay among charge, spin, and orbital degrees of freedom leads to phenomena such as metal–insulator transitions, magnetic phase transitions, and nanoscale charge and orbital ordering. To this effect, pure cubic, perovskite, single-crystalline $La_{0.5}Ba_{0.5}MnO_3$ nanowires (with diameters of 30 to 150 nm and lengths of several to tens of microns) and $La_{1-x}Ba_xMnO_3$ nanocubes (sizes ranging between 50 to 100 nm) have been synthesized by a hydrothermal method at low reaction temperature. Magnetic measurements on the cubes show that their magnetic properties depend on the degree of doping level.[174]

Nanocrystalline electroceramics such as tantalates and niobates are another fascinating class of ABO_3 perovskite materials. For example,[175] single crystalline $NaTaO_3$ nanorods, with aspect ratios varying between 10 and 20:1 and with their long axis oriented in the [010] direction, can be synthesized with high (>90%) yield by reduction of $TaCl_5$

with THF solutions of alkalide $K^+(15\text{-crown-}5)_2Na^-$, followed by annealing of the product under dynamic vacuum (10^{-3} Torr) at 250 °C for 3 h and 600 °C for 4 h. Orthorhombic and rhombohedral single-crystalline potassium niobates with different morphologies have been synthesized through a low-temperature hydrothermal method by simply altering the reaction solvent.[176] A similar hydrothermal processing route[177] produced anisotropic submicrometre particles of $KNbO_3$. Piezoelectric activity, switching polarization, and piezoelectric hysteresis loops were observed in these ferroelectric perovskite nanorods by means of AFM-assisted detection of induced piezoelectric vibrations. Lastly, highly anisotropic nanocrystallites in the form of nanoneedles and nanoplatelets of $KNbO_3$ perovskite were prepared by crystallization of an amorphous gel, which itself was derived from a 'polymerizable-complex method' based on a Pechini-type reaction route. The nanoneedles thereby synthesized were typically 50 nm thick and approximately 10 μm long and had surfaces parallel to the {100} planes of a pseudocubic perovskite structure.[178]

Finally, vanadates are important for usage as catalysts, polarizers, laser host materials, and phosphors. Single-crystalline $NdVO_4$ nanorods,[179] monazite- and zircon-type $LaVO_4$ nanocrystals,[180] and NaV_6O_{15} and $Na_2V_6O_{16}\cdot 3H_2O$ nanowires[181] have all been synthesized under hydrothermal conditions.

7. Summary and outlook

It is clear that ternary metal oxide nanostructures are of fundamental scientific interest (in terms of electronic, optical, and catalytic properties) and possess a broad range of technological applications (including as transistors and computing devices). In the past few years, vast efforts have been expended in the development of new synthetic approaches for these materials at the nanoscale. Indeed the availability of these nanomaterials can provide useful building blocks for enabling the realization of highly efficient and complex nanoscale devices such as NVFRAM memory cells, transducers, actuators, infrared sensors, DRAM storage capacitors, and thermal infrared switches.

Though it is possible to produce ternary oxide nanomaterials with predictable size and/or shape, a few key issues of ternary metal oxide nanostructure synthesis remain to be addressed.

1. For most of the applications associated with ternary oxides at the nanoscale to attain their full potential, generating crystalline nanostructures, with controllable sizes, shapes, and morphologies, on a large scale, using environmentally friendly protocols, represents a very significant experimental challenge. In fact, reproducibly and simultaneously generating control over nanoparticle structure, surface chemistry, monodispersity, crystal structure, and assembly remains an elusive goal.

2. The exact growth mechanisms involved with most of the synthetic methods used for creating ternary oxide nanostructures are often a matter of speculation. For instance, it is empirically known that factors such as temperature, ionic strength, solvent viscosity, as well as the presence of organic ligands play an important role in determining the morphology of the final products. However, the precise mechanism of how each individual variable correlates with overall nanoparticle growth is rarely known. Importantly, it is experimentally nontrivial to probe the growth of these structures kinetically.

3. In addition, properties of nanoscale materials (*e.g.* rods, particles, or arrays of such nanostructures), such as their mechanical, transport, photoconductive, thermoelectric, electronic, optical, and catalytic properties, are theoretically expected to differ from those of the bulk. Little though has been published on property investigations of these nanomaterials due to the relative infancy of the field. Hence, it is very difficult to postulate any precise structure–property correlations at this point.

4. The nature of defects (such as the presence of vacancies and interstitial sites as well as their associated effects on properties) in these systems is not well understood.

5. Potential health and environmental issues associated with these various synthetic protocols of the as-obtained nanomaterials will need to be addressed in a timely fashion.

We believe that future work in this field will continue to focus on generating improved fabrication and synthetic strategies aimed at resolving these issues. Technological advances will arise from multidisciplinary contributions, which will hopefully open up new areas of nanoscience research.

Acknowledgements

We acknowledge support of this work through start-up funds provided by the State University of New York at Stony Brook as well as Brookhaven National Laboratory. In addition, research was supported in part by the US Department of Energy Office of Basic Energy Sciences under Contract DE-AC02-98CH10886 for personnel support and equipment usage. Acknowledgment is also made to the National Science Foundation (DMII-0403859 and CAREER award DMR-0348239), and the donors of the Petroleum Research Fund administered by the American Chemical Society, for PI support of this research. Y. M. recognizes Sigma Xi for a Grant-in-Aid of Research. S. S. W. thanks 3M for a non-tenured faculty award.

References

1 C. M. Lieber, *MRS Bull.*, 2003, **28**, 486.
2 B. L. Cushing, V. L. Kolesnichenko and C. J. O'Connor, *Chem. Rev.*, 2004, **104**, 3893.
3 C. N. R. Rao and A. K. Cheetham, *J. Mater. Chem.*, 2001, **11**, 2887.
4 G. R. Patzke, F. Krumeich and R. Nesper, *Angew. Chem., Int. Ed.*, 2002, **41**, 2446.
5 J. C. Hulteen and C. R. Martin, *J. Mater. Chem.*, 1997, **7**, 1075.
6 G. Schmid, *J. Mater. Chem.*, 2002, **12**, 1231.
7 Z. W. Pan, Z. R. Dai and Z. L. Wang, *Science*, 2001, **291**, 1947.
8 Z. L. Wang, *J. Mater. Chem.*, 2005, **15**, 1021.
9 X.-S. Fang, C.-H. Ye, L.-D. Zhang and T. Xie, *Adv. Mater.*, 2005, **17**, 1661.
10 J. Hu, T. W. Odom and C. M. Lieber, *Acc. Chem. Res.*, 1999, **32**, 435.
11 J. Pérez-Ramirez and B. Vigeland, *Angew. Chem., Int. Ed.*, 2005, **44**, 1112.
12 Y. Xia, P. Yang, Y. Sun, Y. Wu, B. Mayers, B. Gates, Y. Yin, F. Kim and H. Yan, *Adv. Mater.*, 2003, **15**, 353.
13 M. Remškar, *Adv. Mater.*, 2004, **16**, 1497.
14 C. N. R. Rao and M. Nath, *Dalton Trans.*, 2003, 1.
15 R. Tenne, *Chem. Eur. J.*, 2002, **8**, 5296.
16 W. Tremel, *Angew. Chem., Int. Ed.*, 1999, **38**, 2175.
17 Y. Wu, H. Yan, M. Huang, B. Messer, J. H. Song and P. Yang, *Chem. Eur. J.*, 2002, **8**, 1260.

18 Z. A. Peng and X. Peng, *J. Am. Chem. Soc.*, 2002, **124**, 3343.
19 V. F. Puntes, K. M. Krishnan and A. P. Alivisatos, *Science*, 2001, **291**, 2115.
20 M. Mo, J. Zeng, X. Liu, W. Yu, S. Zhang and Y. Qian, *Adv. Mater.*, 2002, **14**, 1658.
21 S. J. Limmer, S. Seraji, M. J. Forbess, Y. Wu, T. P. Chou, C. Nguyen and G. Z. Cao, *Adv. Mater.*, 2001, **13**, 1269.
22 J. K. N. Mbindyo, T. E. Mallouk, J. B. Mattzela, I. Kratochvilova, B. Razavi, T. N. Jackson and T. S. Mayer, *J. Am. Chem. Soc.*, 2002, **124**, 4020.
23 M. Ginzburg-Margau, S. Fournier-Bidoz, N. Coombs, G. A. Ozin and I. Manners, *Chem. Commun.*, 2002, 3022.
24 H. Cölfen and S. Mann, *Angew. Chem., Int. Ed.*, 2003, **42**, 2350.
25 C. N. R. Rao, F. L. Deepak, G. Gundiah and A. Govindaraj, *Prog. Solid State Chem.*, 2003, **31**, 5.
26 T. Trindade, P. O'Brien and N. L. Pickett, *Chem. Mater.*, 2001, **13**, 3843.
27 O. Auciello, J. F. Scott and R. Ramesh, *Phys. Today*, 1998, **51**, 22.
28 I. I. Naumov, L. Bellaiche and H. Fu, *Nature*, 2004, **432**, 737.
29 C. H. Ahn, K. M. Rabe and J.-M. Triscone, *Science*, 2004, **303**, 488.
30 J. F. Scott, *Nat. Mater.*, 2005, **4**, 13.
31 N. A. Hill, *J. Phys. Chem. B*, 2000, **104**, 6694.
32 J. F. Scott, *Ferroelectr. Rev.*, 1998, **1**, 1.
33 T. K. Song, J. Kim and S.-I. Kwun, *Solid State Commun.*, 1996, **97**, 143.
34 A. G. Schrott, J. A. Misewich, V. Nagarajan and R. Ramesh, *Appl. Phys. Lett.*, 2003, **82**, 4770.
35 S. Tao and J. T. S. Irvine, *Nat. Mater.*, 2003, **2**, 320.
36 J. H. Haeni, P. Irvin, W. Chang, R. Uecker, P. Reiche, Y. L. Li, S. Choudhury, W. Tian, M. E. Hawley, B. Craigo, A. K. Tagantsev, X. Q. Pan, S. K. Streiffer, L. Q. Chen, S. W. Kirchoefer, J. Levy and D. G. Schlom, *Nature*, 2004, **430**, 758.
37 K. J. Choi, M. Biegalski, Y. L. Li, A. Sharan, J. Schubert, R. Uecker, P. Reiche, Y. B. Chen, X. Q. Pan, V. Gopalan, L.-Q. Chen, D. G. Schlom and C. B. Eom, *Science*, 2004, **306**, 1005.
38 V. Hornebecq, C. Huber, M. Maglione, M. Antonietti and C. Elissalde, *Adv. Funct. Mater.*, 2004, **14**, 899.
39 H. Fu and L. Bellaiche, *Phys. Rev. Lett.*, 2003, **91**, 257601.
40 P. Padmini and T. R. N. Kutty, *J. Mater. Chem.*, 1994, **4**, 1875.
41 C. Liu, B. Zou, A. J. Rondinone and Z. J. Zhang, *J. Am. Chem. Soc.*, 2001, **123**, 4344.
42 S. O'Brien, L. Brus and C. B. Murray, *J. Am. Chem. Soc.*, 2001, **123**, 12085.
43 J. J. Urban, W. S. Yun, Q. Gu and H. Park, *J. Am. Chem. Soc.*, 2002, **124**, 1186.
44 J. J. Urban, J. E. Spanier, L. Ouyang, W. S. Yun and H. Park, *Adv. Mater.*, 2003, **15**, 423.
45 W. S. Yun, J. J. Urban, Q. Gu and H. Park, *Nano Lett.*, 2002, **2**, 447.
46 S. Wada, H. Chikamori, T. Noma and T. Suzuki, *J. Mater. Sci.*, 2000, **35**, 4857.
47 M. Niederberger, N. Pinna, J. Polleux and M. Antonietti, *Angew. Chem., Int. Ed.*, 2004, **43**, 2270.
48 B. A. Hernandez, K.-S. Chang, E. R. Fisher and P. K. Dorhout, *Chem. Mater.*, 2002, **14**, 480.
49 F. D. Morrison, Y. Luo, I. Szafraniak, V. Nagarajan, R. B. Wehrspohn, M. Steinhart, J. H. Wendroff, N. D. Zakharov, E. D. Mishina, K. A. Vorotilov, A. S. Sigov, S. Nakabayashi, M. Alexe, R. Ramesh and J. F. Scott, *Rev. Adv. Mater. Sci.*, 2003, **4**, 114.
50 Y. Luo, I. Szafraniak, N. D. Zakharov, V. Nagarajan, M. Steinhart, R. B. Wehrspohn, J. H. Wendorff, R. Ramesh and M. Alexe, *Appl. Phys. Lett.*, 2003, **83**, 440.
51 S. J. Limmer, S. Seraji, Y. Wu, T. P. Chou, C. Nguyen and G. Z. Cao, *Adv. Funct. Mater.*, 2002, **12**, 59.
52 S. Han, C. Li, Z. Liu, B. Lei, D. Zhang, W. Jin, X. Liu, T. Tang and C. Zhou, *Nano Lett.*, 2004, **4**, 1241.
53 J. O. Eckert, Jr., C. C. Hung-Houston, B. L. Gersten, M. M. Lencka and R. E. Riman, *J. Am. Ceram. Soc.*, 1996, **79**, 2929.
54 M. M. Lencka and R. E. Riman, *Chem. Mater.*, 1993, **5**, 61.
55 M. Z.-C. Hu, V. Kurian, E. A. Payzant, C. J. Rawn and R. D. Hunt, *Powder Technol.*, 2000, **110**, 2.
56 P. K. Dutta and J. R. Gregg, *Chem. Mater.*, 1992, **4**, 843.
57 C.-T. Xia, E.-W. Shi, W.-Z. Zhong and J.-K. Guo, *J. Cryst. Growth*, 1996, **166**, 961.
58 S. W. Lu, B. I. Lee, Z. L. Wang and W. D. Samuels, *J. Cryst. Growth*, 2000, **219**, 269.
59 Y. Mao, S. Banerjee and S. S. Wong, *Chem. Commun.*, 2003, 408.
60 G. Xu, Z. Ren, P. Du, W. Weng, G. Shen and G. Han, *Adv. Mater.*, 2005, **17**, 907.
61 Y. Mao, S. Banerjee and S. S. Wong, *J. Am. Chem. Soc.*, 2003, **125**, 15718.
62 K. H. Yoon, Y. S. Cho and D. H. Kang, *J. Mater. Sci.*, 1998, **33**, 2977.
63 C. J. Murphy, *Science*, 2002, **298**, 2139.
64 A. Filankembo, S. Giorgio, I. Lisiecki and M. P. Pileni, *J. Phys. Chem. B*, 2003, **107**, 7492.
65 A. Filankembo and M. P. Pileni, *Appl. Surf. Sci.*, 2000, **164**, 260.
66 R. Ranjan, D. Pandey, W. Schuddinck, O. Richard, P. De Meulenaere, J. Van Landuyt and G. Van Tendeloo, *J. Solid State Chem.*, 2001, **162**, 20.
67 S. Qin, A. I. Becerro, F. Seifert, J. Gottsmann and J. Jiang, *J. Mater. Chem.*, 2000, **10**, 1609.
68 R. Ranjan, D. Pandey and N. P. Lalla, *Phys. Rev. Lett.*, 2000, **84**, 3726.
69 Y. Mao and S. S. Wong, *Adv. Mater.*, 2005, **17**, 2194.
70 J. L. Ribeiro, M. T. Lacerda-Arôso, M. R. Chaves, M. Maglione and A. Almeida, *J. Phys.: Condens. Matter*, 1999, **11**, 1247.
71 R. Li, Q. Tang, S. Yin, Y. Yamaguchi and T. Sato, *Chem. Lett.*, 2004, **33**, 412.
72 M. Grätzel, *Nature*, 2001, **414**, 338.
73 M. R. Hoffmann, S. T. Martin, W. Choi and D. W. Bahnemann, *Chem. Rev.*, 1995, **95**, 69.
74 O. K. Varghese, D. Gong, M. Paulose, K. G. Ong, E. C. Dickey and C. A. Grimes, *Adv. Mater.*, 2003, **15**, 624.
75 J. D. Bryan, S. M. Heald, S. A. Chambers and D. R. Gamelin, *J. Am. Chem. Soc.*, 2004, **126**, 11640.
76 C. Xu, Y. Zhan, K. Hong and G. Wang, *Solid State Commun.*, 2003, **126**, 545.
77 X. Sun and Y. Li, *Chem. Eur. J.*, 2003, **9**, 2229.
78 R. Ma, Y. Bando and T. Sasaki, *Chem. Phys. Lett.*, 2003, **380**, 577.
79 T. Sasaki and M. Watanabe, *J. Am. Chem. Soc.*, 1998, **120**, 4682.
80 Q. Wang, Q. Gao and J. Shi, *J. Am. Chem. Soc.*, 2004, **126**, 14346.
81 R. Ma, T. Sasaki and Y. Bando, *J. Am. Chem. Soc.*, 2004, **126**, 10382.
82 S. W. Keller, H.-N. Kim and T. E. Mallouk, *J. Am. Chem. Soc.*, 1994, **116**, 8817.
83 E. R. Kleinfeld and G. S. Ferguson, *Science*, 1994, **265**, 370.
84 Q. Chen, G. H. Du, S. Zhang and L.-M. Peng, *Acta Crystallogr., Sect. B: Struct. Sci.*, 2002, **B58**, 587.
85 Q. Chen, W. Zhou, G. H. Du and L.-M. Peng, *Adv. Mater.*, 2002, **14**, 1208.
86 D. J. D. Corcoran, D. P. Tunstall and J. T. S. Irvine, *Solid State Ionics*, 2000, **136–137**, 297.
87 N. Masaki, S. Uchida and T. Sato, *J. Mater. Sci.*, 2000, **35**, 3307.
88 N. Masaki, S. Uchida, H. Yamane and T. Sato, *Chem. Mater.*, 2002, **14**, 419.
89 M. Tomiha, N. Masaki, S. Uchida and T. Sato, *J. Mater. Sci.*, 2002, **37**, 2341.
90 B. B. Lakshmi, C. J. Patrissi and C. R. Martin, *Chem. Mater.*, 1997, **9**, 2544.
91 B. B. Lakshmi, P. K. Dorhout and C. R. Martin, *Chem. Mater.*, 1997, **9**, 857.
92 H. Imai, Y. Takei, K. Shimizu, M. Matsuda and H. Hirashima, *J. Mater. Chem.*, 1999, **9**, 2971.
93 M. Zhang, Y. Bando and K. Wada, *J. Mater. Sci. Lett.*, 2001, **20**, 167.
94 J. H. Jung, H. Kobayashi, K. J. C. van Bommel, S. Shinkai and T. Shimizu, *Chem. Mater.*, 2002, **14**, 1445.
95 D. Li and Y. Xia, *Adv. Mater.*, 2004, **16**, 1151.
96 T. Kasuga, M. Hiramatsu, A. Hoson, T. Sekino and K. Niihara, *Adv. Mater.*, 1999, **11**, 1307.
97 Z. R. Tian, J. A. Voigt, J. Liu, B. Mckenzie, M. J. Mcdermott, M. A. Rodriguez, H. Konishi and H. Xu, *Nat. Mater.*, 2003, **2**, 821.
98 G. H. Du, Q. Chen, R. C. Che, Z. Y. Yuan and L.-M. Peng, *Appl. Phys. Lett.*, 2001, **79**, 3702.

99 A. R. Armstrong, G. Armstrong, J. Canales and P. G. Bruce, *Angew. Chem., Int. Ed.*, 2004, **43**, 2286.
100 T.-Z. Ren, Z.-Y. Yuan and B.-L. Su, *Colloids Surf., A*, 2004, **241**, 73.
101 H. Zhu, X. Gao, Y. Lan, D. Song, Y. Xi and J. Zhao, *J. Am. Chem. Soc.*, 2004, **126**, 8380.
102 H. Y. Zhu, Y. Lan, X. P. Gao, S. P. Ringer, Z. F. Zheng, D. Y. Song and J. C. Zhao, *J. Am. Chem. Soc.*, 2005, **127**, 6730.
103 A. Thorne, A. Kruth, D. Tunstall, J. T. S. Irvine and W. Zhou, *J. Phys. Chem. B*, 2005, **109**, 5439.
104 R. Ma, K. Fukuda, T. Sasaki, M. Osada and Y. Bando, *J. Phys. Chem. B*, 2005, **109**, 6210.
105 F. Caruso, *Chem. Eur. J.*, 2000, **6**, 413.
106 X. Jiang, T. Herricks and Y. Xia, *Adv. Mater.*, 2003, **15**, 1205.
107 F. Caruso, X. Shi, R. A. Caruso and A. Susha, *Adv. Mater.*, 2001, **13**, 740.
108 T. Nakashima and N. Kimizuka, *J. Am. Chem. Soc.*, 2003, **125**, 6386.
109 H. G. Yang and H. C. Zeng, *J. Phys. Chem. B*, 2004, **108**, 3492.
110 J.-M. Wu, *J. Cryst. Growth*, 2004, **269**, 347.
111 J. S. Raut, P. Bhattad, A. C. Kulkarni and V. M. Naik, *Langmuir*, 2005, **21**, 516.
112 B. Liu and H. C. Zeng, *J. Am. Chem. Soc.*, 2004, **126**, 8124.
113 J. Y. Lao, J. Y. Huang, D. Z. Wang and Z. F. Ren, *J. Mater. Chem.*, 2004, **14**, 770.
114 Z. Zhang, X. Shao, H. Yu, Y. Wang and M. Han, *Chem. Mater.*, 2005, **17**, 332.
115 D. V. Bavykin, V. N. Parmon, A. A. Lapkin and F. C. Walsh, *J. Mater. Chem.*, 2004, **14**, 3370.
116 C. Ederer and N. A. Spaldin, *Nat. Mater.*, 2004, **3**, 849.
117 H. Schmid, *Ferroelectrics*, 1999, **221**, 9.
118 G. A. Smolenskii and I. E. Chupis, *Sov. Phys. Usp. (Engl. Transl.)*, 1982, **25**, 475.
119 F. Kubel and H. Schmid, *Acta Crystallogr., B*, 1990, **B46**, 698.
120 M. Fiebig, Th. Lottermoser, D. Fröhlich, A. V. Goltsev and R. V. Pisarev, *Nature*, 2002, **419**, 818.
121 J. Wang, J. B. Neaton, H. Zheng, V. Nagarajan, S. B. Ogale, B. Liu, D. Viehland, V. Vaithyanathan, D. G. Schlom, U. V. Waghmare, N. A. Spaldin, K. M. Rabe, M. Wuttig and R. Ramesh, *Science*, 2003, **299**, 1719.
122 J. Li, H. He, F. Lü, Y. Duan and D. Song, *Mater. Res. Soc. Symp. Proc.*, 2001, **676**, Y7.7.1.
123 T.-J. Park, Y. Mao and S. S. Wong, *Chem. Commun.*, 2004, 2708.
124 S. Ghosh, S. Dasgupta, A. Sen and H. Sekhar Maiti, *J. Am. Ceram. Soc.*, 2005, **88**, 1349.
125 T.-J. Park and S. S. Wong, 2005, unpublished results.
126 C. R. Martin, *Science*, 1994, **266**, 1961.
127 C. R. Martin, *Acc. Chem. Res.*, 1995, **28**, 61.
128 T. Wada, A. Kajima, M. Inoue, T. Fujii and K. I. Arai, *Mater. Sci. Eng., A*, 1996, **A217–218**, 218, 414.
129 T. Kanai, S. Ohkashi and K. Hashimoto, *J. Phys. Chem. Solids*, 2003, **64**, 391.
130 J. Li, J. Wang, M. Wuttig, R. Ramesh, N. Wang, B. Ruette, A. P. Pyatakov, A. K. Zvezdin and D. Viehland, *Appl. Phys. Lett.*, 2004, **84**, 5261.
131 G. Xu, H. Hiraka, G. Shirane, J. Li, J. Wang and D. Viehland, *Appl. Phys. Lett.*, 2005, **86**, 182905.
132 J. Wang, H. Zheng, Z. Ma, S. Prasertchoung, M. Wuttig, R. Droopad, J. Yu, K. Eisenbeiser and R. Ramesh, *Appl. Phys. Lett.*, 2004, **85**, 2574.
133 K. Y. Yun, M. Noda, M. Okuyama, H. Saeki, H. Tabata and K. Saito, *J. Appl. Phys.*, 2004, **96**, 3399.
134 X. Qi, J. Dho, M. Blamire, Q. Jia, J.-S. Lee, S. Foltyn and J. L. MacManus-Driscoll, *J. Magn. Magn. Mater.*, 2004, **283**, 415.
135 X. Qi, P. S. Roberts, N. D. Mathur, J. S. Lee, S. Foltyn, Q. X. Jia and J. L. MacManus-Driscoll, *Ceram. Trans.*, 2005, **162**, 69.
136 X. Qi, M. Wei, Y. Lin, Q. Jia, D. Zhi, J. Dho, M. G. Blamire and J. L. MacManus-Driscoll, *Appl. Phys. Lett.*, 2005, **86**, 071913.
137 S. Iakovlev, C.-H. Solterbeck, M. Kuhnke and M. Es-Souni, *J. Appl. Phys.*, 2005, **97**, 094901.
138 J. B. Neaton, C. Ederer, U. V. Waghmare, N. A. Spaldin and K. M. Rabe, *Phys. Rev. B: Condens. Matter Mater. Phys.*, 2005, **71**, 014113.
139 A. S. Poghossian, H. V. Abovian, P. B. Avakian, S. H. Mkrtchian and V. M. Haroutunian, *Sens. Actuators, B*, 1991, **4**, 545.
140 N. Shamir, E. Gurewitz and H. Shaked, *Acta Crystallogr., Sect. A: Cryst. Phys., Diffr., Theor. Gen. Cryst.*, 1978, **A34**, 662.
141 N. I. Zakharchenko, *Kinet. Catal.*, 2002, **43**, 95.
142 Y. Xiong, M. Wu, Z. Peng, N. Jiang and Q. Chen, *Chem. Lett.*, 2004, **33**, 502.
143 E. Kostiner and G. L. Shoemaker, *J. Solid State Chem.*, 1971, **3**, 186.
144 T.-J. Park, G. C. Papaefthymiou, A. R. Moodenbaugh, Y. Mao and S. S. Wong, *J. Mater. Chem.*, 2005, **15**, 2099.
145 L. Li and W. Wang, *Solid State Commun.*, 2003, **127**, 639.
146 S.-H. Yu, B. Liu, M.-S. Mo, J.-H. Huang, X.-M. Liu and Y.-T. Qian, *Adv. Funct. Mater.*, 2003, **13**, 639.
147 X.-L. Hu and Y.-J. Zhu, *Langmuir*, 2004, **20**, 1521.
148 P. Černý, P. G. Zverev, H. Jelínková and T. T. Basiev, *Opt. Commun.*, 2000, **177**, 397.
149 P. Černý and H. Jelínková, *Opt. Lett.*, 2002, **27**, 360.
150 M. Nikl, P. Bohacek, E. Mihokova, M. Kobayashi, M. Ishii, Y. Usuki, V. Babin, A. Stolovich, S. Zazubovich and M. Bacci, *J. Lumin.*, 2000, **87–89**, 1136.
151 J. Economy, D. T. Meloon and R. L. Ostrozynski, *J. Catal.*, 1965, **4**, 446.
152 J. Yin, Z. Zou and J. Ye, *Chem. Phys. Lett.*, 2003, **378**, 24.
153 M. Li, H. Schnablegger and S. Mann, *Nature*, 1999, **402**, 393.
154 S. Kwan, F. Kim, J. Akana and P. Yang, *Chem. Commun.*, 2001, 447.
155 F. Kim, S. Kwan, J. Akana and P. Yang, *J. Am. Chem. Soc.*, 2001, **123**, 4360.
156 H. Shi, L. Qi, J. Ma and H. Cheng, *Chem. Commun.*, 2002, 1704.
157 H. Shi, L. Qi, J. Ma, H. Cheng and B. Zhu, *Adv. Mater.*, 2003, **15**, 1647.
158 H. Shi, L. Qi, J. Ma and H. Cheng, *J. Am. Chem. Soc.*, 2003, **125**, 3450.
159 S.-H. Yu, H. Cölfen and M. Antonietti, *Chem. Eur. J.*, 2002, **8**, 2937.
160 S.-H. Yu, M. Antonietti, H. Cölfen and J. Hartmann, *Nano Lett.*, 2003, **3**, 379.
161 S.-H. Yu, H. Cölfen and M. Antonietti, *Adv. Mater.*, 2003, **15**, 133.
162 B. Xie, Y. Wu, Y. Jiang, F. Li, J. Wu, S. Yuan, W. Yu and Y. Qian, *J. Cryst. Growth*, 2002, **235**, 283.
163 Y. Mao and S. S. Wong, *J. Am. Chem. Soc.*, 2004, **126**, 15245.
164 S. V. Dorozhkin, E. I. Dorozhkina and M. Epple, *Cryst. Growth Des.*, 2004, **4**, 389.
165 A. Becker, W. Becker, J. C. Marxen and M. Epple, *Z. Anorg. Allg. Chem.*, 2003, **629**, 2305.
166 O. Grassmann and P. Löbmann, *Biomaterials*, 2004, **25**, 277.
167 K. Schwarz and M. Epple, *Chem. Eur. J.*, 1998, **4**, 1898.
168 M. H. Huang, S. Mao, H. Feick, H. Yan, Y. Wu, H. Kind, E. Weber, R. Russo and P. Yang, *Science*, 2001, **292**, 1897.
169 P. Yang, *Nature*, 2003, **425**, 243.
170 X. Feng, L. Feng, M. Jin, J. Zhai, L. Jiang and D. Zhu, *J. Am. Chem. Soc.*, 2004, **126**, 62.
171 Z. R. Tian, J. A. Voigt, J. Liu, B. Mckenzie and H. Xu, *J. Am. Chem. Soc.*, 2003, **125**, 12384.
172 D. Zhu, H. Zhu and Y. Zhang, *Appl. Phys. Lett.*, 2002, **80**, 1634.
173 T. Zhang, C. G. Jin, T. Qian, X. L. Lu, J. M. Bai and X. G. Li, *J. Mater. Chem.*, 2004, **14**, 2787.
174 J. J. Urban, L. Ouyang, M.-H. Jo, D. S. Wang and H. Park, *Nano Lett.*, 2004, **4**, 1547.
175 J. A. Nelson and M. J. Wagner, *J. Am. Chem. Soc.*, 2003, **125**, 332.
176 J.-F. Liu, X.-L. Li and Y.-D. Li, *J. Nanosci. Nanotechnol.*, 2002, **2**, 617.
177 G. Suyal, E. Colla, R. Gysel, M. Cantoni and N. Setter, *Nano Lett.*, 2004, **4**, 1339.
178 I. Pribosic, D. Makovec and M. Drofenik, *Chem. Mater.*, 2005, **17**, 2953.
179 X. Wu, Y. Tao, L. Dong, J. Zhu and Z. Hu, *J. Phys. Chem. B*, 2005, **109**, 11544.
180 C.-J. Jia, L.-D. Sun, L.-P. You, X.-C. Jiang, F. Luo, Y.-C. Pang and C.-H. Yan, *J. Phys. Chem. B*, 2005, **109**, 3284.
181 G.-T. Zhou, X. Wang and J. C. Yu, *Cryst. Growth Des.*, 2005, **5**, 969.